ACS OMEGA

Article

Cite This: ACS Omega 2019, 4, 22178−22186

http://pubs.acs.org/journal/acsodf

Experimental Investigation of Hydrophobically Modified α-ZrP Nanosheets for Enhancing Oil Recovery in Low-Permeability Sandstone Cores

Hong Chen,*,† Song Qing,† Zhong-bin Ye,† Li-juan Han,‡ Xiao Wang,† Liang Xu,† and Zhao-kun Liu‡

†State Key Laboratory of Oil and Gas Reservoir Geology and Exploitation and ‡School of Chemistry and Chemical Engineering, Southwest Petroleum University, Chengdu 610500, China

ABSTRACT: Highly crystalline α-zirconium phosphate (α-ZrP) nanoparticles were synthesized and exfoliated into nanosheets, and then the hydrophilic nanosheets were modified into hydrophobic nanosheets with octadecyltrichlorosilane (OTS). Scanning electron microscopy, Fourier transform infrared spectroscopy, X-ray diffraction, and thermogravimetric analysis were applied to confirm the morphology and chemical structure of the nanosheets. Contact angle measurement was conducted to explore the wettability alteration of the hydrophobically modified α-ZrP nanosheets, and the result showed that the wettability of the core was changed into hydrophobicity. When ZrP−OTS nanosheets were injected during water-flooding, a Pickering emulsion will be formed. The droplet diameters and viscosities of the Pickering emulsions were measured. The hydrophobically modified α-ZrP nanosheets were applied in low-permeability sandstone cores and various concentrations were tested. The injectivity of the hydrophobically modified α-ZrP nanosheets was also studied and the result indicated that the nanosheets exhibit good injectivity. The mechanisms for enhancing oil recovery by utilizing hydrophobic α-ZrP nanosheets were analyzed: forming Pickering emulsions and increasing the viscosity of the displacing phase. Forming emulsions and increasing the viscosity of the flooding phase can enhance the microdisplacement efficiency, while good injectivity can also enhance the macrodisplacement efficiency. The result indicated the possibility of using hydrophobically modified α-ZrP nanosheets for enhancing oil recovery in a low-permeability reservoir.

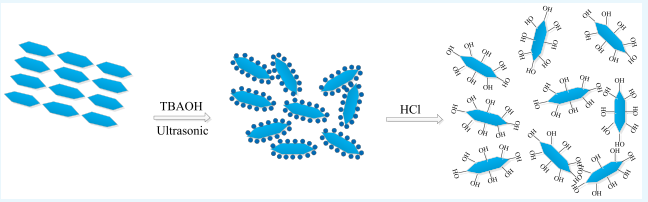

1. INTRODUCTION

Low-permeability reservoirs play a significant and increasing role of oil reserves in the world, but their exploitation always present poor recovery. Hence, lots of methods have been developed to enhance oil recovery; because of the relatively cheap cost and easy operation, water-flooding becomes the reasonable method for the improvement of oil recovery after primary production in low-permeability reservoirs. Other methods such as miscible or immiscible gas injection[1] and nanofilm flooding technology[2] are also popular.

By conducting water-flooding, with the mechanism of maintaining the reservoir pressure and displacing crude oil, the recovery can reach 10−40% of the original oil in place.[3] However, there is still considerable amount of oil detained in the pores after water-flooding, and the reason of this phenomenon can attribute to interfacial and surface forces. For low-permeability reservoirs, the urgent issue is the difficulty of injection and high injecting pressure.

Wettability, as Anderson defined, "the ability of a fluid to spread or adhere to the rock surface in the presence of another immiscible fluid[4]", is a major factor during the process of water-flooding. Some scholars suggested that after long contact with organic components of oil, the surface of rocks is oil-wet in some portions.[5] In the primitive reservoir condition, water injection is relatively easy and the injecting pressure remains stable; however, after long time water-flooding, this situation will be altered. As the front water constantly washes the surface of the pores while conducting water-flooding, the wettability of the pores can be altered into hydrophilicity, and the post water could be hard to inject, for the existence of hydrogen bonds.

Nanotechnology, for the utilization of nanomaterials, can provide many new methods for enhanced oil recovery (EOR).[6−8] Nanoparticles are in the size of 1−100 nm with dimension, and they have unique properties for their small sizes also with a greater surface area per unit volume.[9] Nanoparticles can flow through the pores of the oil reservoirs easily and without any block because of their small size. In addition, with the large surface/volume ratio, nanoparticles can be adsorbed on the surface of pores, which can alter the surface energy and wettability of the system,[10] and also the wettability would affect oil recovery during water-flooding.[11] Chaudhury (2003) and Wasan and Nikolov (2003) first reported that liquids containing nanoparticles can change the wettability of a solid surface.[12,13] Ehtesabi et al. conducted the experiment of using hydrophilic TiO_2 nanoparticles to improve recovery of heavy oil from sandstone cores.[14] Wijayanto et al. conducted the experiment of using hydrophilic aluminosilicate nanoparticles for enhancing waxy crude oil recovery.[15] Numerous

Received: October 18, 2019
Accepted: November 20, 2019
Published: December 12, 2019

DOI: 10.1021/acsomega.9b03481
ACS Omega 2019, 4, 22178−22186

studies have confirmed the ability of nanoparticles to alter porous media into a more water-wet condition.[16−19] All of these methods share the same characteristics, that is, by injecting the hydrophilic nanoparticles, altering the wettability of the core, and reducing the interfacial tension.[20−25] However, the utilization of hydrophobic nanoparticles for enhancing oil recovery has been barely seen in literature studies[26,27] and the mechanism is still ambiguous. In our work, we applied hydrophobic α-ZrP nanomaterials for enhancing oil recovery and analyzed the main mechanisms.

α-Zirconium phosphate (α-ZrP), with the formula of $Zr(HPO_4)_2{\cdot}H_2O$, is characterized for its layered structure and ion-exchange capabilities.[28,29] The size of α-ZrP nanomaterials varies from 50 nm to 2 μm and contains lots of hydroxide groups on the surface.[30] Because of the existence of hydroxide groups, α-ZrP shows the ability of hydrophilicity; hence, hydrophobic alkane is normally the alternative for modification. α-ZrP nanomaterials are usually used as rheological thickeners in many areas such as cosmetics and pharmaceutical products.[31] As a member of lamellar nanomaterials, α-ZrP holds the feature that strong bonds are in the *x* and *y* direction of the plane while weaker ones are in the *z* direction; therefore, guest molecules can achieve intercalation and exfoliation.[32] The interlayer distance of α-ZrP nanomaterials is about 0.76 nm and the thickness of one nanosheet is about 0.66 nm.[33] Therefore, α-ZrP can be exfoliated into monolayers and can be further modified.

In this paper, we first synthesized highly crystalline α-ZrP by the refluxing method and then exfoliated α-ZrP nanomaterials into nanosheets by tetrabutylammonium hydroxide (TBAOH) solution. HCl solution was subsequently added to make α-ZrP regain activity regeneration. After that, octadecyltrichlorosilane (OTS) was used to modify α-ZrP nanosheets from hydrophilicity to hydrophobicity. The results were confirmed by scanning electron microscopy (SEM), transmission electron microscopy (TEM), Fourier transform infrared spectroscopy (FTIR), and X-ray diffraction (XRD). Then, the hydrophobically modified α-ZrP nanosheets were used to conduct the core flooding test in low-permeability sandstone cores, and the experiment results showed that hydrophobic α-ZrP nanosheets had good performance in enhancing oil recovery. The mechanism of this performance was also studied by contact angle measurement, emulsification test, viscosity measurement, SEM, and energy-dispersive spectroscopy (EDS).

2. RESULTS AND DISCUSSION

2.1. SEM and TEM. Figure 1a illustrates the SEM image of pristine α-ZrP nanomaterials which are synthesized by refluxing methods. According to the image, the α-ZrP nanomaterials exhibit a layered structure and less regularly hexagonal shape and one single α-ZrP nanomaterial has the structure with lateral dimensions of about 400 nm. Figure 1b shows the TEM graph of exfoliated α-ZrP nanosheets. In each pristine α-ZrP nanomaterials, there are about 30 layers of nanosheets and each monolayer has a thickness of 0.68 nm.[34,35] The distance between each layer is about 0.76 nm, and each layer is attached with another mostly by a hydrogen bond because of its abundant hydroxyl groups (ca. 4.2 group/nm^2 per side).[36] α-ZrP is a weak inorganic solid acid for it contains medium strong P−OH Brønsted acid groups. TBAOH is most broadly used to exfoliate α-ZrP nanoparticles among various reagents. By reacting with H^+ on the surface of α-ZrP nanoparticles and intercalating into the interlayer, TBAOH solution can exfoliate ZrP nanoparticles into monolayers. The intercalation process of TBA^+ took place first from the edge and then transferred to the internal gallery of layers.[37] Actually, the whole stage can be divided into two steps, first intercalating and then exfoliating. The exfoliation can be regarded as an extreme case of intercalation. However, because of the existence of relatively higher van der Waals forces, the TBA^+ can only partially exfoliate the α-ZrP nanoparticles, so sonication was adopted to achieve full exfoliation. By producing ultrasonic cavitation,[38] which occurs mainly in the frequency range of 100−1000 kHz, use of sonication can result in complete exfoliation (shown in Figure 2).

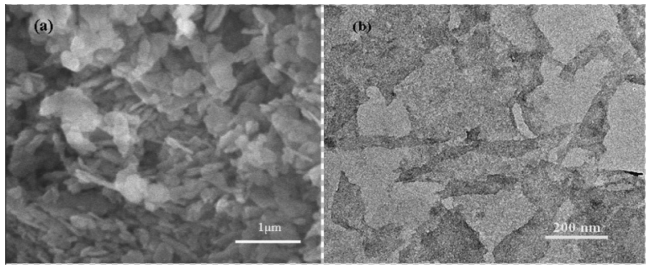

Figure 1. (a) SEM image of α-ZrP nanoparticles and (b) TEM image of exfoliated α-ZrP nanosheets.

2.2. Fourier Transform Infrared Spectroscopy. Figure 3 shows the FTIR spectra of pristine α-ZrP, OTS, and hydrophobically modified α-ZrP (ZrP−OTS). For the pristine α-ZrP, the bands located at 3510 and 3590 cm^{-1} represent the asymmetric and symmetric stretching of the intercalated water, respectively.[39] It can be clearly seen from the spectra of ZrP−OTS, that these two bands had disappeared. It can be attributed to that the full exfoliation removed this crystalline water, which existed in the interlayer. The peaks at 3165 and 1620 cm^{-1} can attribute to symmetric and bending vibrations of −OH groups in α-ZrP, respectively. The bands at 970 and 1251 cm^{-1} are due to the out-of-plane and in-plane vibration of the P−OH groups, respectively. The disappearance of these bands in ZrP−OTS means the successful reaction of Si−Cl and −OH groups. In the spectra of OTS, the bands at 2930 and 2850 cm^{-1} represent the symmetric and asymmetric stretching of CH_2 and CH_3 of the long alkyl chain in OTS, respectively. It can be observed that these two bands appeared in the spectra of ZrP−OTS, suggesting the successful covalent grafting on the surface of α-ZrP.

2.3. X-ray Diffraction. The XRD patterns of α-ZrP nanomaterials and ZrP−OTS are shown in Figure 4. For the pristine α-ZrP, the interlayer space is ca. 0.76 nm,[40] and it can be observed from the pattern, which also indicates the good crystallinity of the α-ZrP nanomaterials, while in the XRD pattern of ZrP−OTS, the main sharp peak disappeared and a new but weak peak appeared at ca. 10.4 Å. When the exfoliation occurred, the crystalline structure of α-ZrP nanomaterials has been totally destroyed, which causes the disappearance of the sharp peak. As the α-ZrP nanosheets get protonated by adding HCl solution, the nanosheets would get restacked and form a gel because of the existence of hydrogen bonds on the −OH groups. When the α-ZrP gel gets dried, recrystallined, and grafted with OTS, the interlayer distance (ca. 10.4 Å) exhibited is larger than the original one (ca. 7.6 Å) because of the existence of long alkyl chains. In the pattern of ZrP−OTS, no sharp diffraction peaks were observed as the α-

DOI: 10.1021/acsomega.9b03481
ACS Omega 2019, 4, 22178−22186

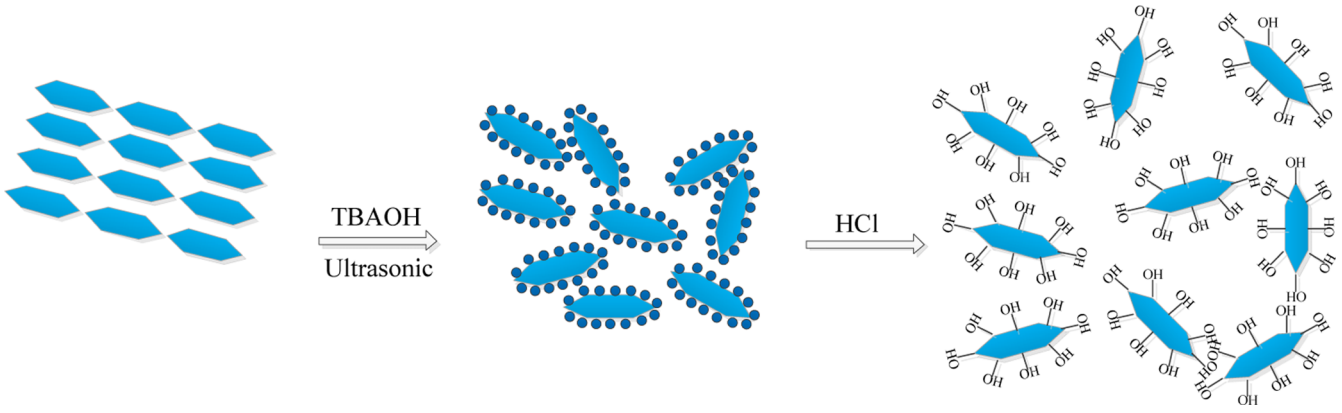

Figure 2. Schematic of the preparation of α-ZrP nanosheets.

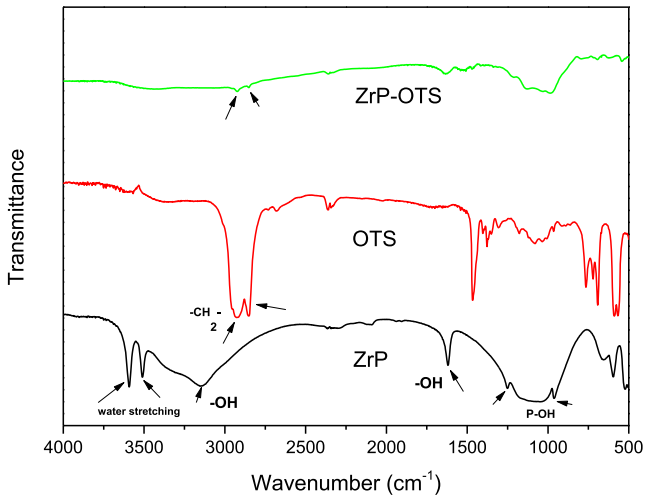

Figure 3. FTIR spectra of α-ZrP, OTS, and ZrP−OTS.

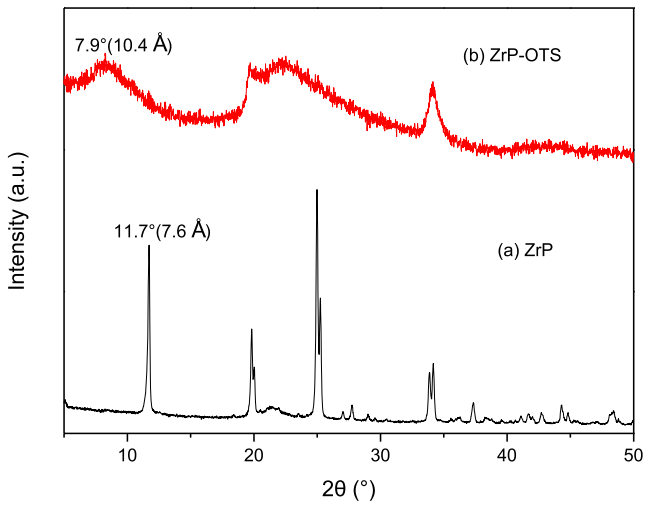

Figure 4. XRD patterns of α-ZrP and ZrP−OTS.

ZrP nanomaterial pattern, which means that the long chain alkane was grafted on the α-ZrP nanosheets in random arrangement and the nanosheets were restacked into a loosely ordered layered structure.

2.4. Thermogravimetric Analysis. The thermal decomposition of the α-ZrP nanomaterials and ZrP−OTS is studied by thermogravimetric analysis (TGA), and the results are shown in Figure 5. Pristine α-ZrP nanomaterials exhibit two major weight losses from 118 to 170 and 506 to 607 °C. From

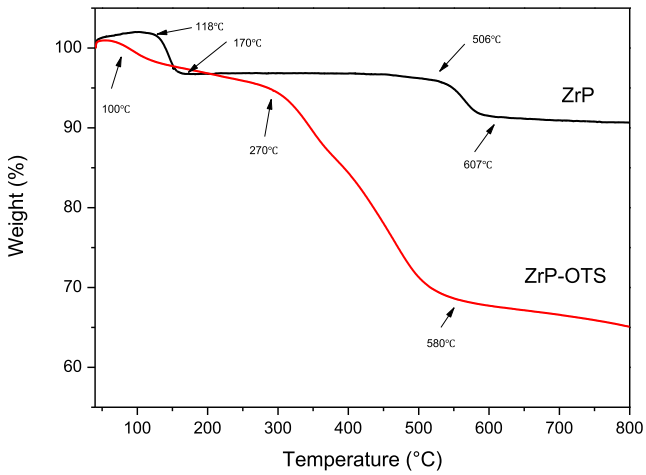

Figure 5. TGA thermograms of ZrP and ZrP−OTS.

118 to 170 °C, the pristine α-ZrP nanomaterials display a weight loss of 3%, which is attributed to the evaporation of the interlayer crystallization water. From 506 to 607 °C, the 5% weight loss is mainly for the dehydration condensation reaction of α-ZrP nanomaterials and the final product is ZrP_2O_7. For the curve of ZrP−OTS, the first weight loss appeared from 40 to 100 °C, which is the loss of the residual solvent on the surface of ZrP−OTS. There is no similar stage from 100 to 170 °C found on the curve of ZrP−OTS, which means that the layered structure has been destructed and the crystallization water has been removed. The next level of ZrP−OTS starts from 270 to 580 °C, which is mainly the removal of the grafted long chain alkane and the condensation of phosphate.

2.5. Wettability Alteration Evaluation. To investigate the wettability alteration ability of the ZrP−OTS nanosheets, different concentrations are prepared with 20, 50, 100, 200, 500, and 1000 mg/L, by dispersing ZrP−OTS into tetrahydrofuran solvents. Hexadecyl trimethyl ammonium bromide (CTAB) solution (25 mg/L) is also prepared to test its effect. Then, the hydrophilic core slices, polished by sandpaper first, are soaked in the ZrP−OTS dispersed system and 25 mg/L CTAB solution for 24 h and dried overnight. To avoid the nanosheet aggregation, the slices are placed vertically so that the ZrP−OTS nanosheets can be absorbed on the surface of the slice freely. After that, the contact angle of the

DOI: 10.1021/acsomega.9b03481
ACS Omega 2019, 4, 22178−22186

slice is measured, and the result is shown in Figure 6. The original core slice is highly hydrophilic; when the water is

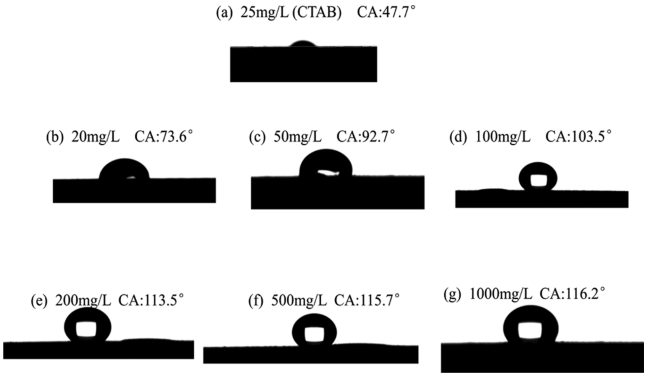

Figure 6. Contact angle of the core slice surface: (a) contact angle of 25 mg/L CTAB; (b–g) contact angle of ZrP–OTS with different concentrations.

dropped on the surface of the slice, it will immediately permeate into the slice, so the original core surface is highly hydrophilic. Figure 6a shows that the slice is still hydrophilici (CA: 47.7°) which meant that adding of 25 mg/L CTAB exerts few influences. It can be clearly seen from Figure 6b–g that when the slice is soaked in 20 mg/L, the contact angle is 73.6°, higher than the original one while still hydrophilici. It can be attributed to the reason that when the concentration is low, there are not enough nanomaterials that are absorbed on the surface of the slice, and the slice can only partially exhibit hydrophobicity. When the concentrations are higher, 50 and 100 mg/L, it can be seen that the contact angle increased correspondingly to 92.7 and 103.5°. This phenomenon indicates that as the concentration is getting higher, more and more ZrP–OTS nanosheets are absorbed on the surface of the slice and alter the wettability of the slice from hydrophilicity to hydrophobicity. However, when the concentrations further increased (200, 500, and 1000 mg/L), the contact angle (113.5, 115.7, and 116.2°) did not increase significantly. It can be attributed to that when enough amount of hydrophobic ZrP–OTS nanosheets are absorbed on the slice, and because of the specific surface energy, the nanosheets will fully cover the slice and then will not further alter the wettability of the slice.

2.6. Emulsification Test and Viscosity Measurement.

Pickering emulsion is an emulsion stabilized by solid particles.[41] Compared with classical emulsion, normally stabilized by a surfactant, Pickering emulsion has a specific property. High resistance to coalescence is a major benefit of Pickering emulsion.[42] The existence of ZrP–OTS nanosheets allows the stabilization of droplets as small as few micrometers. Figure 7a shows the optical microscopic image of water and crude oil with 25 mg/L CTAB, and Figure 7b shows the image of water and crude oil (the mass ratio of water/oil is 1/1). It can be seen that the diameters of the droplet as shown in Figure 7a ranged from 10 to 20 μm and as shown in Figure 7b ranged from 50 to 100 μm. However, both of the emulsions were not stable. When ZrP–OTS nanosheets were added in the system (Figure 7c–f), the solid nanosheets were adsorbed onto the water/oil interface, and the surface energy reduced, which led to the stabilization of the emulsion. The droplet diameters decreased with the increase of ZrP–OTS. When the concentrations of ZrP–OTS are low (20 and 50 mg/L), the diameters of the droplet ranged between 20 and 30 μm. When the concentration is 100 mg/L, the diameter of the droplet was about 10 μm. However, when the concentration was higher (500 mg/L), the diameter did not decrease obviously. When the ZrP–OTS nanosheets are added during the water-flooding process, w/o Pickering emulsion can be formed and thus will enhance the fluidity of the oil.

The viscosities of water and crude oil are 1.08 and 9.76 mPa·s, respectively, which are measured by using a Brookfield viscosimeter. The viscosities of emulsified oil with different ZrP–OTS concentrations are shown in Table 1. It can be seen that the viscosities of emulsified oil are between those of water and crude oil.

Table 1. Viscosities of Emulsified Oil with Different ZrP–OTS Concentrations

number	concentration (mg/L)	viscosity (mPa·s)
1	20	4.57
2	50	5.14
3	100	5.87
4	200	6.14
5	500	6.24

2.7. Injectivity Study of ZrP–OTS Nanosheets.

Nanomaterials have a good effect when applied for EOR; however, nanomaterials are easy to get accumulated and cause blockage

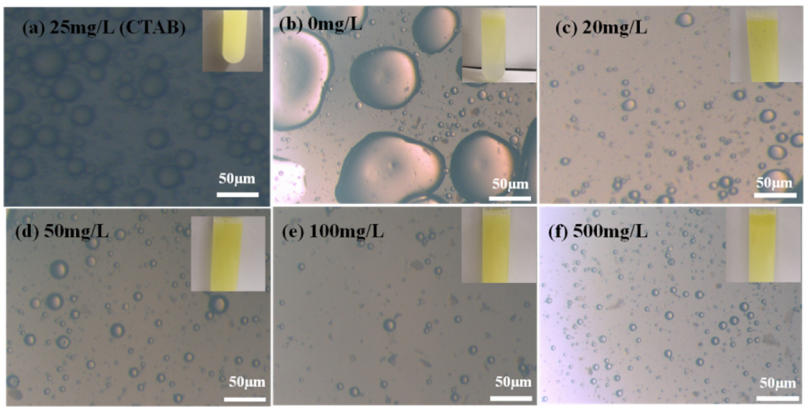

Figure 7. Optical microscope image of emulsions; (a) CTAB of 25 mg/L; (b–f) ZrP–OTS nanosheets with different concentrations.

DOI: 10.1021/acsomega.9b03481
ACS Omega 2019, 4, 22178–22186

Table 2. Parameters of Cores for the Injectivity Study

number	size (cm)	pore volume (cm^3)	porosity (%)	permeability ($\times 10^{-3}$ μm^2)	injecting rate (mL/min)	injecting concentration (mg/L)
1	Φ 2.5 × 6.41	6.17	19.61	21.79	0.10	25 (CTAB)
2	Φ 2.5 × 6.47	6.03	18.9	22.3	0.10	20
3	Φ 2.5 × 6.45	6.18	19.5	24.8	0.10	50
4	Φ 2.5 × 6.43	6.05	19.2	26.7	0.10	100
5	Φ 2.5 × 6.49	6.21	19.5	25.9	0.10	200
6	Φ 2.5 × 6.41	6.12	19.4	23.5	0.10	500

in the pore. This phenomenon is more serious in low-permeability reservoirs, so it is necessary to study the injectivity of ZrP−OTS nanosheets. Five different concentrations of ZrP−OTS nanosheets are prepared to study the injectivity. CTAB (25 mg/L) is also prepared to study its influence. The parameters of the sandstone cores are shown in Table 2, and the flooding pressures before and after injection are shown in Table 3 and Figure 8, respectively.

Table 3. Flooding Pressures before and after ZrP−OTS Injection

number	injecting concentration (mg/L)	water-flooding pressure (MPa)	ZrP−OTS flooding pressure (MPa)
1	10 (CTAB)	1.6149	1.6214
1	20	1.5941	1.5609
2	50	1.6012	1.5161
3	100	1.5849	1.4515
4	200	1.6104	1.4342
5	500	1.6097	1.4189

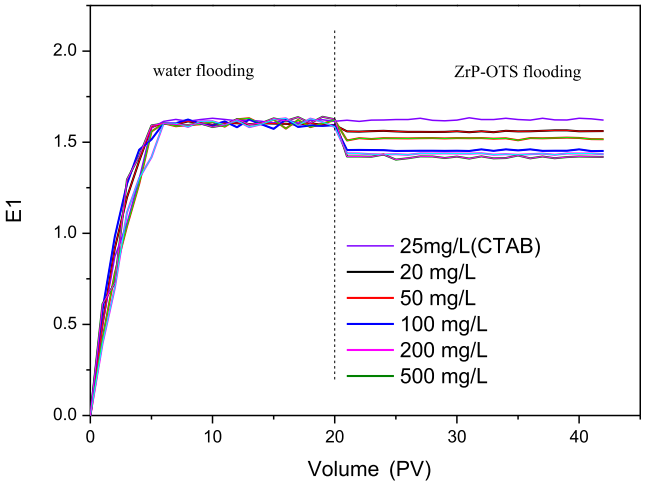

Figure 8. Flooding pressures before and after 25 mg/L and ZrP−OTS with different concentrations of injections.

It can be observed from Table 3 and Figure 8 that the flooding pressure stabled about 1.6 MPa. When 25 mg/L CTAB solution is injected, the injecting pressure is barely changed, which means that the CTAB exerted few influences in the flooding process for its weaker hydrophobicity than ZrP−OTS nanosheets. When the ZrP−OTS solution is injected, the injecting pressure decreases obviously. When the injecting concentration is 50 mg/L, the flooding pressure decreases to 1.56 MPa, and when the injecting pressure is 500 mg/L, the flooding pressure decreases to 1.41 MPa. This indicates that the blockage phenomenon did not occur. The results indicate that the ZrP−OTS nanosheets have excellent injectivity.

To understand the mechanism, the core slice was studied by SEM and EDS. Figure 9 shows the morphology of the core

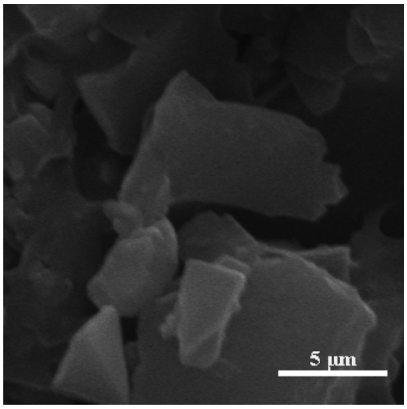

Figure 9. SEM image of the core before flooding.

surface before flooding. The pores of the core can be clearly seen and the size of the pore tunnel lies in the micrometer scale. When ZrP−OTS solution is injected, only part of the surface is deposited with ZrP−OTS nanosheets. As previously tested (Figure 6), different ZrP−OTS concentrations displayed different wettability alteration abilities. When the concentration is low (20 mg/L), only a small amount of ZrP−OTS nanosheets is adsorbed on the surface of the core and only sporadic nanosheets can be found in the SEM image as shown in Figure 10a; also, only a very small portion of Zr is detected in the EDS scanning (Figure 10b). When the concentration is higher (500 mg/L), it can be clearly seen that few layers of ZrP−OTS nanosheets are deposited on the surface of the core (Figure 11a) and the Zr element took a larger portion than before (Figure 11b). The Zr element is deposited homogenously on the surface of the pore (Figure 12). However, the ZrP−OTS nanosheets did not cause blockage because of their thin layered structure.

The system potential energy is reduced when ZrP−OTS nanosheets are adsorbed on the surface, which enable the absorption to be more stable. As the ZrP−OTS nanosheets transformed the wettability of the surface from hydrophilicity into hydrophobicity, during the water-flooding process, there is layered density distribution of water molecules, and the density is smaller when the surface is hydrophilic, for the reduction of potential energy. In addition, the nonuniform density distribution near the surface still exists, which makes the average density reduce and format the low density layer of the hydrophobic surface. When the potential energy between water and core surface, as the surface exhibits hydrophobic, there is obvious slippage effect existing,[43,44] which plays important role in the injecting pressure reducing. With the unique layered structure, the ZrP−OTS nanosheets can exhibit long detention

DOI: 10.1021/acsomega.9b03481
ACS Omega 2019, 4, 22178−22186

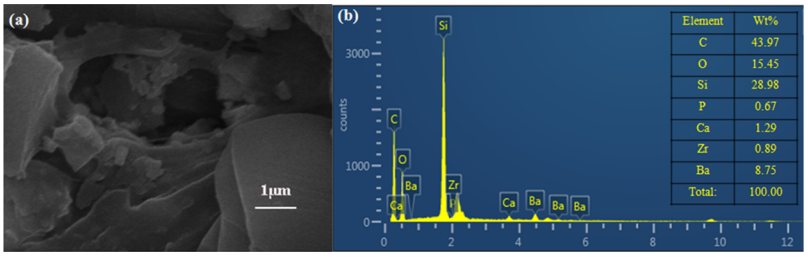

Figure 10. (a) SEM image of the core flooded by 20 mg/L ZrP−OTS solution and (b) EDS measurement of the core after flooding by 20 mg/L ZrP−OTS solution.

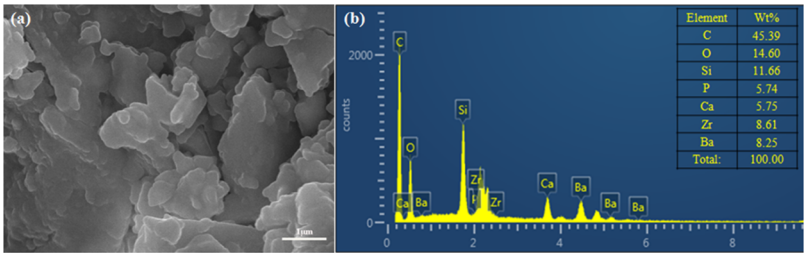

Figure 11. (a) SEM image of the core flooded by 500 mg/L ZrP−OTS solution and (b) EDS measurement of the core after flooding by 500 mg/L ZrP−OTS solution.

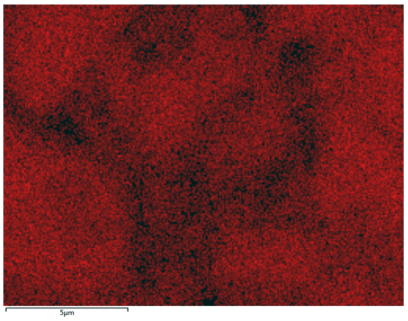

Figure 12. EDS map of Zr after flooding with 500 mg/L ZrP−OTS.

time after long time water-flooding and will not cause apparent blockage in the long-range injection.

2.8. Core Flooding Experiment. Five different concentrations are used to evaluate the ZrP−OTS nanosheets' ability for EOR and the parameters of the core are shown in Table 4. The oil recovery efficiencies before and after injecting ZrP−OTS nanosheets are shown in Table 5.

Table 5 shows the increase in oil recovery as the ZrP−OTS nanosheet concentrations increase. When ZrP−OTS nanosheets are injected into the core and encounter oil, a stabilized w/o Pickering emulsion will be formed during the water-flooding process, as previous analysis. The w/o Pickering emulsion can increase the microdisplacement efficiency (E_D) by enhancing the fluidity of the oil phase. Conversely, the Pickering emulsion, as the flooding phase, with the decreasing fluidity compared with pristine water, can enhance the macrodisplacement efficiency (E_v) by reducing the mobility ratio.

The effect of good injectivity can enhance the macrodisplacement efficiency (E_v) by increasing the sweep efficiency. The overall displacement efficiency

$$E = E_V E_D$$

Hence, the macrodisplacement efficiency (E_v) and microdisplacement efficiency (E_D) both are enhanced and the overall displacement efficiency can subsequently get enhanced.

When the ZrP−OTS nanosheets are injected, the Pickering emulsion is formed, and the Pickering emulsion becomes the new displacing phase fluid. As the viscosity (μ_D) of the Pickering emulsion is higher than that of the previous one (water, 1 mPa·s), the mobility ratio

$$M = \lambda_D/\lambda_d = \frac{K_D}{K_d}\frac{\mu_d}{\mu_D}$$

where λ_D is the mobility of the displacing phase, λ_d is the mobility of the displaced phase, K_D is the permeability of the displacing phase, K_d is the permeability of the displaced phase, μ_D is the viscosity of the displacing phase, and μ_d is the viscosity of the displaced phase. When the viscosity of the displacing phase (μ_D) increases, the mobility ratio (M) will decrease. The decrease in the mobility ratio (M) will increase the sweep efficiency (E_v) and retard the vicious fingering phenomenon.

Table 4. Parameters of Cores for the Flooding Test

number	size (cm)	pore volume (cm^3)	porosity (%)	permeability ($\times 10^{-3}$ μm^2)	injecting concentration (mg/L)
1	Φ 2.5 × 7.16	6.03	17.16	29	20
2	Φ 2.5 × 7.21	6.18	17.47	25	50
3	Φ 2.5 × 7.18	6.05	17.17	24	100
4	Φ 2.5 × 7.23	6.21	17.50	26	200
5	Φ 2.5 × 7.19	6.12	17.34	25	500

DOI: 10.1021/acsomega.9b03481
ACS Omega 2019, 4, 22178−22186

Table 5. Oil Recovery Efficiencies before and after Injecting ZrP−OTS Nanosheets

number	injecting concentration (mg/L)	injecting volume (PV)	water-flooding recovery (%)	ZrP−OTS flooding recovery (%)	post water flooding recovery (%)	overall recovery (%)
1	20	2	26.53	2.37	10.92	39.82
2	50	2	26.78	2.46	12.81	42.05
3	100	2	27.17	2.59	14.36	44.12
4	200	2	26.79	2.54	15.7	45.03
5	500	2	27.22	2.49	17.4	47.11

This result reveals the possibility of using hydrophobically modified α-ZrP nanosheets for EOR after water-flooding in the low-permeability core. Water-flooding is the mostly applied method for improving oil recovery because of its relatively cheap cost. α-ZrP nanoparticles, as inexpensive and environmentally friendly materials, have unique properties compared with other nanomaterials. The combination of water-flooding and α-ZrP nanomaterials may open a new door for petroleum exploitation.

3. CONCLUSIONS

In this paper, highly crystalline α-ZrP nanoparticles are successfully synthesized and subsequently exfoliated into nanosheets. OTS is used to modify α-ZrP nanosheets into hydrophobic. Then, the injectivity of ZrP−OTS nanosheets is studied. The flooding pressures before and after ZrP−OTS injection are measured, which indicate obvious depressurization during the flooding process. SEM and EDS show that the nanosheets are deposited on the slice uniformly. The performance of hydrophobically modified α-ZrP nanosheets for EOR in a low-permeability core is studied. The recovery efficiency can be improved 19% after applying hydrophobic α-ZrP nanosheets. Contact angle measurement implied that nanosheet adsorption changed the wettability of the core slice. The diameter of the Pickering emulsion droplet is measured, and the result indicates that the diameter decreases as the nanosheet concentration increases. However, when the concentration exceeds 100 mg/L, the diameter will not change significantly. The viscosity of the Pickering emulsion was also measured and the result shows that the viscosity increased. As the displacing phase fluid, the increasing viscosity of the w/o Pickering emulsion can decrease the mobility ratio (M) and increase the sweep efficiency (E_v). In summary, hydrophobically modified α-ZrP nanosheets show the possibility for EOR. Being environmentally friendly and low cost, α-ZrP nanomaterials have a promising prospect for commercialized industry EOR materials.

4. MATERIALS AND METHODS

4.1. Synthesis of α-ZrP Nanoparticles. The α-ZrP nanomaterials were synthesized by the refluxing method.[45] First, 9.66 g of $ZrOCl_2{\cdot}8H_2O$ was dissolved in 5 mL of deionized water, and then 60 mL of 12 mol/L H_3PO_4 was added dropwise in the solution with continuous stirring at room temperature. Then, the mixed system was stirred and refluxed at 100 °C for 24 h. After the reaction, the product was centrifuged and rinsed three times with deionized water to remove the excess H_3PO_4 and dried overnight at 65 °C. Then, the product was ground with a mortar and pestle into fine powder to get highly crystalline α-ZrP powder.

4.2. Preparation of Single-Layer α-ZrP Nanosheets. α-ZrP (1 g) was dispersed in 100 mL of deionized water, and then 30 mL of 0.1 mol/L TBAOH (the molar ratio of α-ZrP/TBAOH is 1) solution was added dropwise to reach a constant pH of 8.0. Care was taken to avoid higher pH conditions, otherwise it can lead to rapid corrosion of the sheets.[33] The colloidal suspension was subsequently treated with 100 kHz ultrasonication for 4 h to achieve full exfoliation. After the colloidal suspension was turned into solution of clarity and transparency, 30 mL of 0.1 mol/L HCl (the same molar of TBAOH) was added dropwise, and then the gelatinous precipitate of α-ZrP nanosheets was collected by centrifugation and washed with deionized water until the chloride ions were fully removed (silver nitrate solution was used to confirm the result). The α-ZrP nanosheet gel was then rinsed with acetone three times to exchange the gel from water to acetone; subsequently, the nanosheet gel was washed with toluene following the previous procedure, which ultimately transports the α-ZrP nanosheet gel into toluene solvent with the assistance of ultrasonication.

4.3. Hydrophobic Modification of α-ZrP Nanosheets. The prepared α-ZrP nanosheet gel was dispersed in 50 mL of toluene solvent, and then 1 mL of OTS solution was added into the system. The mixed system was placed at 30 °C for 3 h with mild stirring, and then the product was centrifuged and washed three times with absolute ethanol. The obtained modified α-ZrP was dried overnight at 65 °C and ground into powder (labeled as ZrP−OTS).

4.4. Injectivity Study and Core Flooding Experiment. ZrP−OTS nanosheets were dispersed in deionized water by adding a few amount of CTAB(5 wt % ZrP−OTS nanosheets, and the maximum 25 mg/L CTAB solution was also employed to study its influence) with the assistance of an FJ200-S homogenizer at 10 000 rpm for 2 min and ultrasonication. Different concentrations of ZrP−OTS-dispersed solutions were prepared. To study the injectivity of ZrP−OTS nanosheets, the low-permeability manmade core was flooded by deionized water to measure its water-flooding pressure. In addition, the ZrP−OTS dispersed solution was injected into the core and the ZrP−OTS flooding pressure was obtained. Another group of cores was applied for the EOR experiment. First, the core was saturated with brine water and then with crude oil and aged for 48 h. Then, brine water was used to flood the core until no more oil was produced. Subsequently, ZrP−OTS of 2 PV dispersed solution was injected, and then post water-flooding was conducted until no more oil existed (the schematic of the core flooding experiment is shown in Figure 13).

4.5. Characterizations. SEM was performed by using a field emission scanning electron microanalyzer (FEI Quanta 450) at an accelerating voltage of 20 kV to observe the morphology and the micropores of α-ZrP nanoparticles and the micropores. FTIR by using Thermo Fisher Scientific Nicolet 6700 ranging from 800 to 4000 cm^{-1} was implemented to analyze the chemical composition of pristine α-ZrP nanoparticles, OTS, and modified α-ZrP nanosheets. XRD

DOI: 10.1021/acsomega.9b03481
ACS Omega 2019, 4, 22178−22186

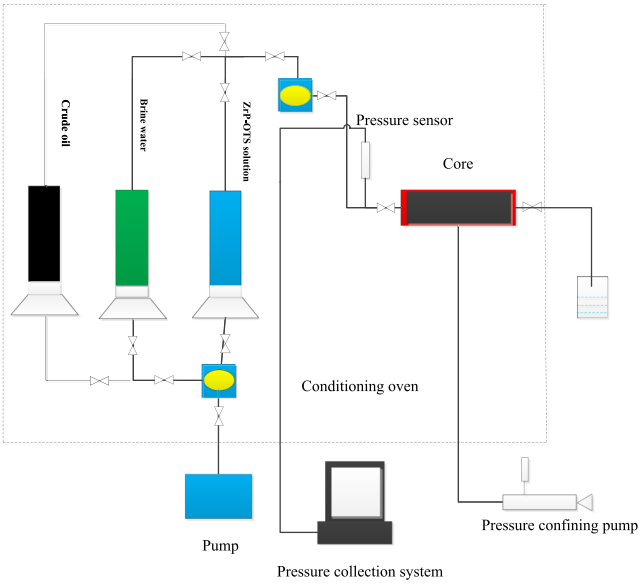

Figure 13. Schematic of the core flooding experiment.

measurement was applied to detect the crystal structure of pristine α-ZrP nanoparticles and ZrP−OTS by using a PANalytical X'Pert-Pro diffractometer (40 kV, 40 mA) with Cu (λ = 1.54 Å) irradiation at a scanning rate of 2 °/s in the 2θ range of 4−40°, and the scan compensation is 20 °/min. TGA was carried out using a NETZSCH simultaneous thermal analyzer model STA 449F3 and with a heating rate of 10 °C/min from 40 to 800 °C in an aluminum crucible under an inert gas atmosphere.

AUTHOR INFORMATION

Corresponding Author

*E-mail: 7445611@qq.com.

ORCID

Hong Chen: 0000-0002-7389-1313

Notes

The authors declare no competing financial interest.

ACKNOWLEDGMENTS

We would like to appreciate the financial support from the National Natural Science Foundation of China (grant no. 51674210).

REFERENCES

(1) Delamaide, E.; Tabary, R.; Rousseau, D. Chemical EOR in low permeability reservoirs. *Proceedings of SPE EOR Conference at Oil Gas West Asia*: Muscat, Oman, March 31−April 2, 2014.

(2) Cheraghian, G.; Hendraningrat, L. A review on applications of nanotechnology in the enhanced oil recovery part A: effects of nanoparticles on interfacial tension. *Int. Nano Lett.* **2016**, *6*, 129−138.

(3) Sohal, M. A.; Thyne, G.; Søgaard, E. G. Review of Recovery Mechanisms of Ionically Modified Waterflood in Carbonate Reservoirs. *Energy Fuels* **2016**, *30*, 1904−1914.

(4) Anderson, W. G. Wettability literature survey-part 3: the effects of wettability on the electrical properties of porous media. *J. Pet. Technol.* **1986**, *38*, 1371−1378.

(5) Salathiel, R. A. Oil Recovery by Surface Film Drainage In Mixed-Wettability Rocks. *J. Pet. Technol.* **1973**, *25*, 1216−1224.

(6) Skauge, T.; Hetland, S.; Spildo, K.; Skauge, A. Nano-sized particles for EOR. *SPE 129933, Proceedings of SPE Improved Oil Recovery Symposium*: Oklahoma, USA, April 24−28, 2010.

(7) Cheraghian, G. An experimental study of a surfactant polymer for enhanced heavy-oil recovery using a glass micromodel by adding nanoclay. *Pet. Sci. Technol.* **2015**, *33*, 1410−1417.

(8) Cheraghian, G.; Khalili Nezhad, S. S.; Kamari, M.; Hemmati, M.; Masihi, M.; Bazgir, S. Effect of nanoclay on improved rheology properties of polyacrylamide solutions used in enhanced oil recovery. *J. Pet. Explor. Prod. Technol.* **2015**, *5*, 189−196.

(9) Singh, S.; Ahmed, R. Vital role of nanopolymers in drilling and stimulations fluid applications. *Paper SPE 130413. Proceedings of SPE Annual Technical Conference and Exhibition*: Florence, Italy, Sept 19−22, 2010.

(10) Ayatollahi, S.; Zerafat, M. M. Nanotechnology-assisted EOR techniques: New solutions to old challenges. *Proceedings of the SPE International Oilfield Nanotechnology Conference*: Noordwijk, Netherlands, June 12−14, 2012.

(11) Anderson, W. G. Wettability Literature Survey-Part 6: The Effects of Wettability on Waterflooding. *J. Pet. Technol.* **1987**, *39*, 1605−1622.

(12) Chaudhury, M. K. Spread the Word about Nanofluids. *Nature* **2003**, *423*, 131.

(13) Wasan, D. T.; Nikolov, A. D. Spreading of Nanofluids on Solids. *Nature* **2003**, *423*, 156.

(14) Ehtesabi, H.; Ahadian, M. M.; Taghikhani, V.; Ghazanfari, M. H. Enhanced Heavy Oil Recovery in Sandstone Cores Using TiO_2 Nanofluids. *Energy Fuels* **2014**, *28*, 423−430.

(15) Wijayanto, T.; Kurihara, M.; Kurniawan, T.; Muraza, O. Experimental Investigation of Aluminosilicate Nanoparticles for Enhanced Recovery of Waxy Crude Oil. *Energy Fuels* **2019**, *33*, 6076−6082.

(16) Mohammed, M. A.; Babadagli, T. Experimental Investigation of Wettability Alteration in Oil-Wet Reservoirs Containing Heavy Oil. *Proceedings of SPE Heavy Oil Conference*: Calgary, June 10−12, 2016.

(17) Roustaei, A. An Evaluation of Spontaneous Imbibition of Water into Oil-Wet Carbonate Reservoir Cores Using Nanofluid. *Petrophysics* **2014**, *55*, 31−37.

(18) Cao, N.; Mohammed, M. A.; Babadagli, T. Wettability Alteration of Heavy-Oil-Bitumen-Containing Carbonates by Use of Solvents, High-PH Solutions, and Nano/Ionic Liquids. *Proceedings of the Offshore Technology Conference*: Rio de Janeiro, Brazil, Oct 27−29, 2015.

(19) Cheraghian, G.; Hendraningrat, L. A Review on Applications of Nanotechnology in the Enhanced Oil Recovery Part A: Effects of Nanoparticles on Interfacial Tension. *Int. Nano Lett.* **2016**, *6*, 129−138.

(20) Alomair, O. A.; Matar, K. M.; Alsaeed, Y. H. Nanofluids Application for Heavy Oil Recovery. *Proceedings of the SPE Asia Pacific Oil & Gas Conference and Exhibition*: Adelaide, Australia, Oct 14−16, 2014.

(21) Hendraningrat, L.; Shidong, L.; Torsaeter, O. A Glass Micromodel Experimental Study of Hydrophilic Nanoparticles Retention for EOR Project. *Proceedings of the SPE Russian Oil and Gas Exploration and Production Technical Conference and Exhibition*: Moscow, Russia, Oct 16−18, 2012.

(22) Li, S.; Genys, M.; Wang, K.; Torsæter, O. Experimental Study of Wettability Alteration during Nanofluid Enhanced Oil Recovery Process and Its Effect on Oil Recovery. *Proceedings of the SPE Reservoir Characterisation and Simulation Conference and Exhibition*: Abu Dhabi, UAE, Sept 14−16, 2015.

(23) Li, S.; Hendraningrat, L.; Torsaeter, O. Improved Oil Recovery by Hydrophilic Silica Nanoparticles Suspension: 2 Phase Flow Experimental Studies. *Proceedings of the International Petroleum Technology Conference*: Beijing, China, March 26−28, 2013.

(24) Li, S.; Torsæter, O. Experimental Investigation of the Influence of Nanoparticles Adsorption and Transport on Wettability Alteration for Oil Wet Berea Sandstone. *Proceedings of the SPE Middle East Oil & Gas Show and Conference*: Manama, Bahrain, March 8−11, 2015.

(25) Shahrabadi, A.; Bagherzadeh, H.; Roostaie, A.; Golghanddashti, H. Experimental Investigation of HLP Nanofluid Potential to Enhance Oil Recovery: A Mechanistic Approach. *Proceedings of the*

DOI: 10.1021/acsomega.9b03481
ACS Omega 2019, 4, 22178−22186

SPE International Oilfield Nanotechnology Conference and Exhibition: Noordwijk, Nerthelands, 2012.
(26) Ahmadi, M.-A.; Ahmad, Z.; Phung, L. T. K.; Kashiwao, T.; Bahadori, A. Evaluation of the ability of the hydrophobic nanoparticles of SiO_2 in the EOR process through carbonate rock samples. *Pet. Sci. Technol.* **2016**, *34*, 1048−1054.
(27) Chen, H.; Xiao, L.; Xu, Y.; Zeng, X.; Ye, X.-B. A novel nanodrag reducer for low permeability reservoir water flooding: long-chain alkylamines modified graphene oxide. *J. Nanomater.* **2016**, *2016*, 1−9.
(28) Phillips, H. O.; Kraus, K. A. adsorption on inorganic materials. iv. cation exchange properties of zirconium antimonate. *J. Am. Chem. Soc.* **1962**, *84*, 2267−2268.
(29) Amphlett, C. B.; Mcdonald, L. A.; Redman, M. J. Synthetic inorganic ion-exchange materials—i zirconium phosphate. *J. Inorg. Nucl. Chem.* **1958**, *6*, 220−235.
(30) Zhou, Y.; Huang, R.; Ding, F.; Brittain, A. D.; Liu, J.; Zhang, M.; Xiao, M.; Meng, Y.; Sun, L. Sulfonic acid-functionalized alpha-zirconium phosphate single-layer nanosheets as a strong solid acid for heterogeneous catalysis applications. *ACS Appl. Mater. Interfaces* **2014**, *6*, 7417−7425.
(31) Boek, E. S.; Coveney, P. V.; Lekkerkerker, H. N. W.; van der Schoot, P. Simulating the rheology of dense colloidal suspensions using dissipative particle dynamics. *Phys. Rev. E: Stat. Phys., Plasmas, Fluids, Relat. Interdiscip. Top.* **1997**, *55*, 3124−3133.
(32) Martí, A. A.; Colón, J. L. Direct Ion Exchange of Tris(2,2′-bipyridine)ruthenium(II) into an α-Zirconium Phosphate Framework. *Inorg. Chem.* **2003**, *42*, 2830−2832.
(33) Kim, H.-N.; Keller, S. W.; Mallouk, T. E.; Schmitt, J.; Decher, G. Characterization of zirconium phosphate/polycation thin films grown by sequential adsorption reactions. *Chem. Mater.* **1997**, *9*, 1414−1421.
(34) Wang, X.; Zhang, L.; Yu, Y.; Jia, L.; Sam Mannan, M.; Chen, Y.; Cheng, Z. Nano-encapsulated PCM via Pickering Emulsification. *Sci Rep.* **2015**, *5*, 13357.
(35) Mejia, A. F.; Diaz, A.; Pullela, S.; Chang, Y.-W.; Simonetty, M.; Carpenter, C.; et al. Pickering emulsions stabilized by amphiphilic nano-sheets. *Soft Matter* **2012**, *8*, 10245.
(36) Troup, J. M.; Clearfield, A. Mechanism of ion exchange in zirconium phosphates. 20. refinement of the crystal structure of. alpha.-zirconium phosphate. *Inorg. Chem.* **1977**, *16*, 3311−3314.
(37) Sun, L.; Boo, W. J.; Sun, D.; Clearfield, A.; Sue, H.-J. Preparation of Exfoliated Epoxy/α-Zirconium Phosphate Nanocomposites Containing High Aspect Ratio Nanoplatelets. *Chem. Mater.* **2007**, *19*, 1749−1754.
(38) Miller, M. W.; Miller, D. L.; Brayman, A. A. A review of in vitro bioeffects of inertial ultrasonic cavitation from a mechanistic perspective. *Ultrasound Med. Biol.* **1996**, *22*, 1131−1154.
(39) Huisken, F.; Kaloudis, M.; Kulcke, A. Infrared Spectroscopy of Small Size-selected Water Clusters. *J. Chem. Phys.* **1996**, *104*, 17−25.
(40) Sun, L.; Boo, W. J.; Browning, R. L.; Sue, H.-J.; Clearfield, A. Effect of Crystallinity on the Intercalation of Monoamine in Alphazirconium Phosphate Layer Structure. *Chem. Mater.* **2005**, *17*, 5606−5609.
(41) Aveyard, R.; Binks, B. P.; Clint, J. H. Emulsions stabilized solely by solid colloidal particles. *Adv. Colloid Interface Sci.* **2003**, *100-102*, 503−546.
(42) Chevalier, Y.; Bolzinger, M.-A. Emulsions stabilized with solid nanoparticles: Pickering emulsions. *Colloids Surf., A* **2013**, *439*, 23−34.
(43) Bing-Yang, C.; Min, C.; Zeng-Yuan, G. Velocity slip of liquid flow in nanochannels. *Acta Phys. Sin.* **2006**, *55*, 5305−5306.
(44) Khilar, K. C.; Fogler, H. S. Practical Consequences of Release and Migration of Fines in Porous Media. *Migrations of Fines in Porous Media. Theory and Applications of Transport in Porous Media*; Springer: Dordrecht, 1998; Vol. *12*, pp 1−8.
(45) Zhongbin, Y.; Lei, C.; Hong, C.; Lijuan, H.; Qingyuan, C.; Daming, W. α-zirconium phosphate nanocrystals with various morphology for photocatalysis. *Chem. Phys. Lett.* **2018**, *709*, 96−102.

DOI: 10.1021/acsomega.9b03481
ACS Omega 2019, 4, 22178−22186